Enhancing computational steel solidification by a nonlinear transient thermal model

Fatima-Ezzahrae Moutahir[1], Youssef Belhamadia[2], Mofdi El-Amrani[1], and Mohammed Seaid[3]

[1] Mathematics and Applications Laboratory, FST, Abdelmalek Essaadi University, Tangier, Morocco
[2] Department of Mathematics and Statistics, American University of Sharjah, Sharjah, United Arab Emirates
[3] Department of Engineering, University of Durham, South Road, DH1 3LE, UK

Abstract. Designing efficient steel solidification methods could contribute to a sustainable future manufacturing. Current computational models, including physics-based and machine learning-based design, have not led to a robust solidification design. Predicting phase-change interface is the crucial step for steel solidification design. In the present work, we propose a simplified model for thermal radiation to be included in the phase-change equations. The proposed model forms a set of nonlinear partial differential equations and it accounts for both thermal radiation and phase change in the design. As numerical solver we implement a fully implicit time integration scheme and a Newton-type algorithm is used to deal with the nonlinear terms. Computational results are presented for two test examples of steel solidification. The findings here could be used to understand effect of thermal radiation in steel solidification. Combining the present approach with physics-based computer modeling can provide a potent tool for steel solidification design.

Keywords: Steel solidification · Phase change · Thermal radiation · Computational design.

1 Introduction

Melting and solidification processes are natural phenomena and occur in many industrial processes such as crystal growth, continuous casting and metal welding among others. During solidification the phase front travels at the interface between the liquid and solid materials. In all applications that involve high temperature, radiation is expected to greatly influence the thermal features and it cannot be neglected. Experimental predictions of the impact of radiation in materials during the solidification process can be very demanding and laborious. Although the new development of modern engineering technologies, accurate prediction of effects of radiative heat transfer in this type of phase-change materials still faces several complex issues and can be experimentally demanding and challenging. It is well-known that any experimental system intended for investigation always involves meticulous design and subsequent procurement of

ICCS Camera Ready Version 2022
To cite this paper please use the final published version:
DOI: 10.1007/978-3-031-08751-6_22

materials, fabrication or construction of the system, which necessitates heavy financial resources and involves practically more time, see for instance [1–3]. Hence, computational simulations are commonly preferred for designing, modelling and simulation of thermal systems. This numerical investigation helps to accumulate functional data, and identify operating conditions or environment at which the best performance of a workable system could be obtained. Computational simulations therefore can play a crucial role and provide accurate and effective thermal predictions in this class of applications. The present work aims to develop robust computational tools for highly accurate simulations of steel solidification processes.

Many developed methods considered mathematical models based on the enthalpy formulation for simulating the phase-change in the materials. These types of phase change models have been coupled with the natural convection and the mechanical deformation to account for the fluid flow dynamics and internal cracks respectively (see [4], [5], [6], [7], [8] among others). Existence of a weak solution of heterogeneous Stefan problem using enthalpy formulation is presntedn in [9]. Coupling radiation with phase-change models is very complicated and highly demanding. A full radiative heat transfer model consists of an integro-differential equations that are spatially, spectrally, and directionally dependent [10, 11]. These equations are therefore extremely difficult to solve, especially when coupled with the energy transport equation and phase-change closures. However, for optically thick materials with high scattering effects, the thermal radiation can be well approximated with the Rosseland model proposed in [12]. This simplification significantly reduces the computational costs compared to solving the full radiative heat transfer model, see for example [13]. In the present study, we are interested in coupling a class of phase-change models [14, 15] with the Rosseland diffusion approximation of radiative heat transfer. The phase change model employed is considered as intermediate formulation between the enthalpy and the so-called phase-field formulations, where a phase parameter that takes constant values in the solid and liquid phases is employed. The Rosseland approximation includes thermal radiation into the system through a nonlinear diffusion term with convective boundary conditions. The coupled system is expected to provide an accurate representation for radiation transport in both participating and non-participating optically thick media. For the numerical solution of the coupled Rosseland-phase-change model, we propose a consistent finite difference method using staggered grids. The Newton's method is employed to deal with the non-linearity in the mathematical model and two-dimensional numerical results are presented for two test examples to illustrate the effects of radiation on the steel solidification.

This paper is organized as follows. In section 2 we introduce the mathematical equations used for modelling steel solidification. Formulation of the proposed fully implicit method is presented in section 3. Section 4 is devoted to numerical results for two test examples for steel solidification problems. Concluding remarks are presented in Section 5.

ICCS Camera Ready Version 2022
To cite this paper please use the final published version:
DOI: 10.1007/978-3-031-08751-6_22

2 Mathematical models for steel solidification

In general applications, modelling steel solidification involves a computational domain $\Omega = \Omega_l(t) \cup \Omega_s(t) \cup \Gamma(t)$ with time-dependent liquid domain $\Omega_l(t)$, solid domain $\Omega_s(t)$ and the interface $\Gamma(t)$ between both domains. The material properties are expected to vary from one state to another according for the interface location. In this case, the set of governing equations is difficult to solve and one way to overcome the numerical difficulties is to use a new formation over the entire computational domain Ω. In the current work, we reformulate the system using the enthalpy formulation and the semi-phase-field technique described in [14, 15] among others. Thus, given a bounded two-dimensional domain $\Omega \subset \mathbb{R}^2$ with Lipschitz continuous boundary $\partial\Omega$ and a time interval $[0, \mathcal{T}]$, we focus on solving the time-dependent heat equation coupled with the phase change

$$\begin{aligned} \eta(\phi)\frac{\partial T}{\partial t} + \rho L \frac{\partial F_\epsilon(T)}{\partial t} - \nabla \cdot \left(\mathcal{K}_c\left(\phi\right)\nabla T\right) = 0, \qquad & (\mathbf{x}, t) \in \Omega \times [0, \mathcal{T}], \\ \mathcal{K}_c(\phi)\mathbf{n}(\hat{\mathbf{x}}) \cdot \nabla T + \hbar_c(\phi)(T - T_b) = 0, \qquad & (\hat{\mathbf{x}}, t) \in \partial\Omega \times [0, \mathcal{T}], \\ T(\mathbf{x}, 0) = T_0(\mathbf{x}), \qquad & \mathbf{x} \in \Omega, \end{aligned} \tag{1}$$

where $\mathbf{n}(\hat{\mathbf{x}})$ denotes the outward normal in $\hat{\mathbf{x}}$ with respect to $\partial\Omega$, $T(x, t)$ is the temperature field, T_b the boundary temperature, T_0 the initial temperature, ρ the density, L the latent heat of fusion and ϕ is the regularized phase-field function defined as

$$\phi = F_\epsilon(T) = \frac{1}{2} - \frac{1}{2}\tanh\left(\frac{T_f - T}{\epsilon}\right),$$

with T_f is the melting temperature and ϵ is a small parameter selected such that the resulting function F_ϵ is differentiable. In (1),

$$\eta(\phi) = \rho_s c_s + \phi\left(\rho_l c_l - \rho_s c_s\right), \qquad \mathcal{K}_c(\phi) = K_s + \phi\left(K_l - K_s\right),$$

uation

$$\hbar_c(\phi) = \hbar_s + \phi\left(\hbar_l - \hbar_s\right), \qquad \alpha(\phi) = \alpha_s + \phi\left(\alpha_l - \alpha_s\right),$$

where ρ_i, c_i, K_i, $\hbar_i$ and α_i are respectively, the density, specific heat, thermal conductivity, convective heat transfer coefficient and hemispheric emissivity of the phase i with subscripts s and l refer to the solid and liquid phases.

In the present study, to enhance steel solidification modelling we include thermal radiation in grey optically thick media. For a weakly semitransparent medium with large scattering such as steel, an asymptotic expansion for the radiative transfer equation yields the equilibrium diffusion or the Rosseland approximation [12]. When coupled to the phase change equations (1), the Rosseland approximation yields

$$\begin{aligned} \eta(\phi)\frac{\partial T}{\partial t} + \rho L \frac{\partial F_\epsilon(T)}{\partial t} - \nabla \cdot \left(\mathcal{K}_r\left(\phi\right)\nabla T\right) = 0, \qquad & (\mathbf{x}, t) \in \Omega \times [0, \mathcal{T}], \\ \mathcal{K}_c(\phi)\mathbf{n}(\hat{\mathbf{x}}) \cdot \nabla T + \hbar_c(\phi)(T - T_b) = \alpha(\phi)\pi\left(B(T_b) - B(T)\right), \qquad & \\ T(\mathbf{x}, 0) = T_0(\mathbf{x}), \qquad & \mathbf{x} \in \Omega, \end{aligned} \tag{2}$$

ICCS Camera Ready Version 2022
To cite this paper please use the final published version:
DOI: 10.1007/978-3-031-08751-6_22

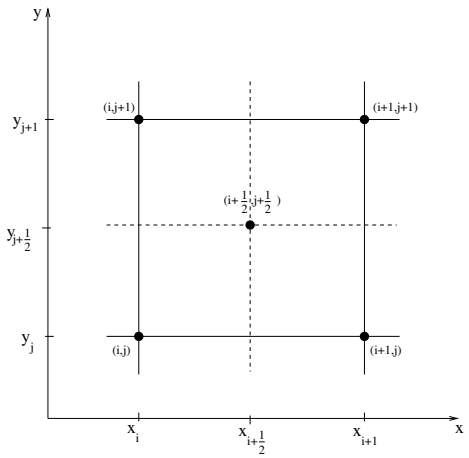

Fig. 1. The staggered grid used for the space discretization.

where $B(T)$ is the spectral intensity of the black-body radiation defined by the Planck function as

$$B(T) = \sigma_R T^4,$$

with $\sigma_R = 5.67 \times 10^{-8}$ is the Stefan-Boltzmann constant. Here, the conduction coefficient $\mathcal{K}_t\,(T)$ is defined as a function of the temperature by

$$\mathcal{K}_r\,(\phi) = \mathcal{K}_c(\phi) + \frac{4\pi}{3\kappa(\phi)}\frac{\partial B}{\partial T},$$

where κ is the absorption coefficient. It should be stressed that the Rosseland approach is widely accepted as an accurate model for radiation transport in both participating and non-participating optically thick media. These equations do not have analytical solutions for phase change and their numerical solutions lead to computationally demanding problems due to the nonlinear diffusion and the presence of internal and external thermal boundary layers.

3 Numerical methods for the nonlinear system

Different numerical methods can be used for solving systems (1) and (2) (see chapter 4 in [16]). The convergence analysis of iterative methods resulted from implicit time discretization of the enthpay formulation coupled with finite difference of the space variables is studied in [17]. Since it is easier to combine upwinding with finite volume discretization than other methods, we consider in this study a space discretization based on volume control and cell averaging. For the time integration we implement a fully implicit backward second-order scheme allowing for large stability in the simulations. Hence, we divide the time

ICCS Camera Ready Version 2022
To cite this paper please use the final published version:
DOI: 10.1007/978-3-031-08751-6_22

interval into subintervals $[t_n, t_{n+1}]$ of equal length Δt and $t_n = n\Delta t$. For simplicity, we discretize the spatial domain into cells with sizes $(\Delta x)_i$ and $(\Delta y)_j$ in the x and y directions, respectively. We also define the maximum cell size $h = \max_{ij}((\Delta x)_i, (\Delta y)_j)$ and the averaged gridpoints as shown in Figure 1 by

$$(\Delta x)_{i+\frac{1}{2}} = x_{i+1} - x_i, \qquad (\Delta y)_{j+\frac{1}{2}} = y_{j+1} - y_j,$$

$$x_{i+\frac{1}{2}} = \frac{x_{i+1} + x_i}{2}, \qquad y_{j+\frac{1}{2}} = \frac{y_{j+1} + y_j}{2}.$$

Using the notation W_{ij}^n to denote the approximation value of the function W at time $t = t_n$ and the gridpoint (x_i, y_j), the semi-discrete form of the system (2) reads

$$\eta(\phi^{n+1}_{i+\frac{1}{2}j+\frac{1}{2}})\mathcal{D}_t^2 T^{n+1}_{i+\frac{1}{2}j+\frac{1}{2}} + \rho L \mathcal{D}_t^2 \phi^{n+1}_{i+\frac{1}{2}j+\frac{1}{2}} - \mathcal{D}_h^2 \left(\mathcal{K}_r T\right)^{n+1}_{ij} = 0, \tag{3}$$

where the temporal difference $\mathcal{D}_t^2$ is defined as

$$\mathcal{D}_t^2 W^{n+1} = \frac{3W^{n+1} - 4W^n + W^{n-1}}{2\Delta t},$$

and the spatial difference operator $\mathcal{D}_h^2$ is given by $\mathcal{D}_h^2 = \mathcal{D}_x^2 + \mathcal{D}_y^2$ with

$$\mathcal{D}_x^2(\mathcal{K}W)_{ij} = \frac{\mathcal{K}_{i,j} + \mathcal{K}_{i+1j}}{2}\frac{W_{i+1j} - W_{ij}}{(\Delta x)^2_{i+\frac{1}{2}}} - \frac{\mathcal{K}_{t_{i-1j}} + \mathcal{K}_{ij}}{2}\frac{W_{ij} - W_{i-1j}}{(\Delta x)^2_{i+\frac{1}{2}}},$$
$$\mathcal{D}_y^2(\mathcal{K}W)_{ij} = \frac{\mathcal{K}_{i,j} + \mathcal{K}_{ij+1}}{2}\frac{W_{ij+1} - W_{ij}}{(\Delta y)^2_{j+\frac{1}{2}}} - \frac{\mathcal{K}_{ij-1} + \mathcal{K}_{ij}}{2}\frac{W_{ij} - W_{ij-1}}{(\Delta y)^2_{j+\frac{1}{2}}},$$

with the cell averages of a function W are given by

$$\begin{aligned} W_{i+1j} &= \frac{1}{(\Delta x)_{i+\frac{1}{2}}}\int_{y_j}^{y_{j+1}} W(x_i, y)dy, \\ W_{ij+1} &= \frac{1}{(\Delta y)_{j+\frac{1}{2}}}\int_{x_i}^{x_{i+1}} W(x, y_j)dx, \\ W_{ij} &= \frac{1}{(\Delta x)_{i+\frac{1}{2}}(\Delta y)_{j+\frac{1}{2}}}\int_{x_i}^{x_{i+1}}\int_{y_j}^{y_{j+1}} W(x, y)dxdy. \end{aligned} \tag{4}$$

Here, the function value of $W_{i+\frac{1}{2}j+\frac{1}{2}}$ at the cell centre is simply approximated by bilinear interpolation as

$$W_{i+\frac{1}{2}j+\frac{1}{2}} = \frac{W_{ij} + W_{i+ij} + W_{ij+1} + W_{i+1j+1}}{4},$$

and the discrete phase-field function $\phi^{n+1}_{i+\frac{1}{2}j+\frac{1}{2}}$ in (3) is defined by

$$\phi^{n+1}_{i+\frac{1}{2}j+\frac{1}{2}} = F_\epsilon\left(T^{n+1}_{i+\frac{1}{2}j+\frac{1}{2}}\right).$$

ICCS Camera Ready Version 2022
To cite this paper please use the final published version:
DOI: 10.1007/978-3-031-08751-6_22

Algorithm 1

1: Given $\mathcal{F}$, tolerance τ and initial guess $T^{(0)}$ chosen to be the solution at the previous time step, the Newton-GMRES algorithm for solving (2) uses the following steps: (we denote by GMRES($\mathcal{A}$,$\mathbf{q}$,$\mathbf{z}^{(0)}$,τ) the result of GMRES algorithm applied to linear system $\mathcal{A}\mathbf{z} = \mathbf{q}$ with initial guess $\mathbf{z}^{(0)}$ and tolerance τ).

2: **for** $k = 0, 1, \ldots$ **do**

3: Compute the residual

$$\mathcal{H}(T^{(k)}) = T^{(k)} - \mathcal{F}(T^{(k)}).$$

4: Solve using GMRES

$$\mathbf{d}^{(k)} = \text{GMRES}\big(\mathcal{H}'(T^{(k)}), -\mathcal{H}(T^{(k)}), \mathbf{d}^{(0)}, \tau^{(k)}\big).$$

5: Update the solution

$$T_L^{(k+1)} = T^{(k)} + \xi \mathbf{d}^{(k)}.$$

6: Check the convergence

$$\text{if} \quad \left(\|T^{(k+1)}\|_{L^2} \leq \tau\right) \qquad \text{stop.}$$

7: **end for**

Similarly, the gradient in the boundary condition in (2) is approximated by upwinding without using ghost points. For example, on the left boundary of the domain, the boundary discretization is

$$-\mathcal{K}_c\left(\phi^{n+1}_{\frac{1}{2}j+\frac{1}{2}}\right)\frac{T^{n+1}_{\frac{3}{2}j+\frac{1}{2}} - T^{n+1}_{\frac{1}{2}j+\frac{1}{2}}}{(\Delta x)_{\frac{1}{2}}} + \hbar_c\left(\phi^{n+1}_{\frac{1}{2}j+\frac{1}{2}}\right)\left(T^{n+1}_{\frac{1}{2}j+\frac{1}{2}} - T_b\right) = \alpha\left(\phi^{n+1}_{\frac{1}{2}j+\frac{1}{2}}\right)\pi\left(B(T_b) - B\left(T^{n+1}_{\frac{1}{2}j+\frac{1}{2}}\right)\right), \quad (5)$$

and similar work has to be done for the other boundaries. All together, the above discretization leads to a nonlinear system reformulated as a fixed point problem for the temperature T as

$$T = \mathcal{F}(T). \quad (6)$$

The Newton's method applied to (6) results in the following iteration

$$T^{(k+1)} = T^{(k)} - \mathcal{H}'\big(T^{(k)}\big)^{-1}\mathcal{H}\big(T^{(k)}\big), \quad (7)$$

where $\mathcal{H}'_L$ is the system Jacobian approximated by a difference quotient of the form

$$\mathcal{H}'\big(T^{(k)}\big)\mathbf{w} \approx \frac{\mathcal{H}\big(T^{(k)} + \delta\mathbf{w}\big) - \mathcal{H}\big(T^{(k)}\big)}{\delta}. \quad (8)$$

If a GMRES method [18] is used to compute the Newton's direction then, at each time step Algorithm 1 is carried out to update the solution T^{n+1}. Here $\|\cdot\|_{L^2}$ denotes the discrete L^2-norm. The Newton step ξ, the tolerance $\tau^{(k)}$ to

ICCS Camera Ready Version 2022
To cite this paper please use the final published version:
DOI: 10.1007/978-3-031-08751-6_22

Table 1. Convergence results for the accuracy example using different time steps Δt at time $t = 1$.

Δt	L^∞-error	Rate	L^1-error	Rate	L^2-error	Rate
0.2	1.1140E-01	—	1.0460E-01	—	7.0500E-02	—
0.1	3.1200E-02	1.8361	2.9300E-02	1.8359	1.9700E-02	1.8394
0.05	8.1000E-03	1.9456	7.6000E-03	1.9468	5.1000E-03	1.9496
0.025	2.0000E-03	2.0179	1.9000E-03	2.0000	1.3000E-03	1.9720

Table 2. Convergence results for the accuracy example using different space steps $h = \Delta x = \Delta y$ at time $t = 1$.

h	L^∞-error	Rate	L^1-error	Rate	L^2-error	Rate
0.2	6.2000E-03	—	6.3000E-03	—	6.4000E-03	—
0.1	8.9546E-04	2.7916	9.8414E-04	2.6553	1.2000E-03	2.4150
0.05	2.1259E-04	2.0746	2.3479E-04	2.0675	2.8667E-04	2.0656
0.025	5.3530E-05	1.9897	5.9890E-05	1.9710	1.8668E-05	2.0162

stop the inner iterations in GMRES, and the difference increment δ in (8) are selected according to backtracking linesearch, Eisenstat-Walker and Hardwired techniques. We refer to [19] for detailed discussions on these techniques. Three to five Newton's iterations were necessary to achieve convergence with a residual norm less than 10^{-6}. The choice of above mentioned time discretization is based on our previous experience [20], where this scheme provided better numerical solutions for other type of interface problems. It should be noted that when using unifrom structured meshes, the above spatial discterization is equivalent to the well-established central finite difference which provides good numerical results.

4 Results and discussions

In this section, we present numerical results for the proposed Rosseland-phase-change simplified model to examine the effect of radiation in materials under phase change. Two test problems are considered to demonstrate the performance of the proposed method. We first start with a manufactured solution to study the convergence of our algorithm. Then, the effect of radiation on the temperature distributions is examined in two solidification examples in the process of continuous casting of steel.

4.1 Accuracy example

As a first test example, we consider a two-dimensional analytical solution to discuss the order of convergence in space and time of the proposed method. Since the analytical solution does not represent a specific physical meaning, we take

ICCS Camera Ready Version 2022
To cite this paper please use the final published version:
DOI: 10.1007/978-3-031-08751-6_22

Table 3. Thermophysical parameters used for the steel solidification.

$\mathcal{K}_c$	34 W/mK
c	691 J/KgK
ρ	7400 Kg/m^3
L	272000 J/Kg
T_f	1809 K
T_0	2000 K
T_b	300 K
h_c	1648.5 $J/(Kg\,K)$
κ	10 m^{-1}
α	0.0001

only numerical values without considering any units. The problem is solved in a squared domain $\Omega = [0,1] \times [0,1]$ subject to boundary and the initial conditions explicitly calculated such that the analytical solution of (1) is given by

$$T_{ex}(t,x,y) = e^{-t^2-x^2-y^2}.$$

The nonlinear diffusion coefficient is given by

$$K_c(\phi) = T^2.$$

We consider the following relative $L^\infty-$, L^1- and L^2-error norms

$$\| e \|_{L^\infty} = \frac{\|T - T_{ex}\|_{L^\infty}}{\|T_{ex}\|_{L^\infty}}, \quad \| e \|_{L^1} = \frac{\|T - T_{ex}\|_{L^1}}{\|T_{ex}\|_{L^1}}, \quad \| e \|_{L^2} = \frac{\|T - T_{ex}\|_{L^2}}{\|T_{ex}\|_{L^2}},$$

where T is the numerical solution and T_{ex} is the analytical solution computed at the final time $t = 1$. First, to test the convergence of the time discretization scheme, we consider four time steps of different sizes using a fine uniform mesh with $\Delta x = \Delta y = 0.002$. The obtained results are listed in Table 1 along with their corresponding convergence rates. Similarly, to examine the convergence of the spatial discretization we consider four space steps of different sizes using a fine time step $\Delta t = 0.0001$. The obtained results are listed in Table 2. As it can be seen the proposed method preserves the second-order accuracy for both space and time for this test problem.

4.2 Steel solidification: Case 1

In all applications that involve high temperature, radiation is expected to greatly influence the thermal features and it cannot be neglected. In this example, we will examine the effect of radiation on the temperature profile in a solidification example during the process of continuous casting of steel. The mathematical model (1) is used to simulate the solidification examples without radiation while, the presence of radiation is simulated using the proposed simplified Rosseland-phase-change model (2). In this first case, we consider a square 0.3 $m \times 0.3$ m

ICCS Camera Ready Version 2022
To cite this paper please use the final published version:
DOI: 10.1007/978-3-031-08751-6_22

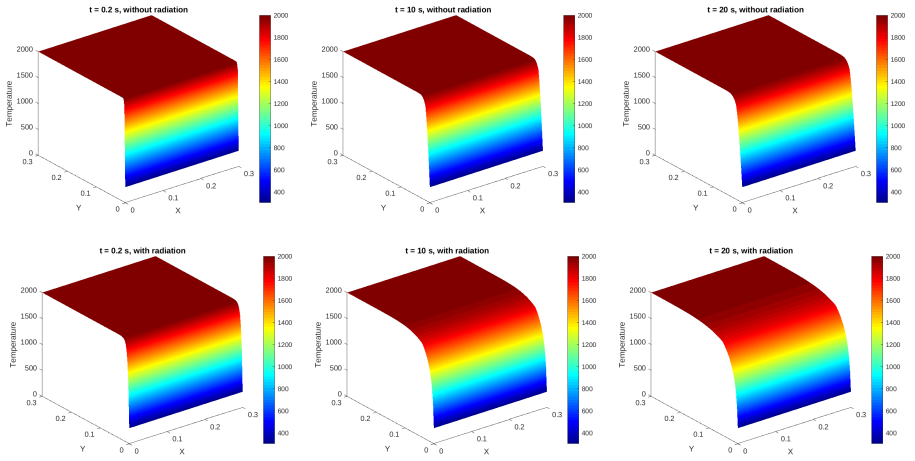

Fig. 2. Temperature without radiation (first row) and with radiation (second row) obtained for Case 1 at time $t = 0.2\ s$ (first column), $t = 10\ s$ (second column) and $t = 20\ s$ (third column).

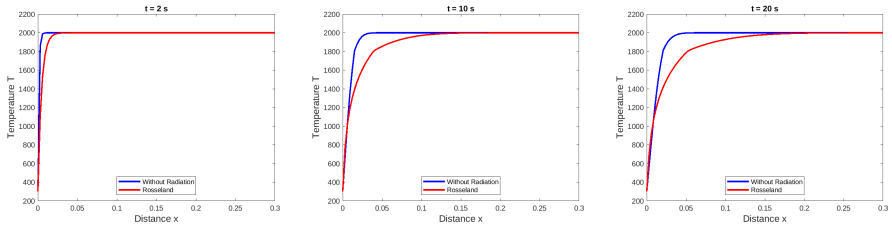

Fig. 3. Cross-sections of the temperature with and without radiation along the horizontal centerline for Case 1 at time $t = 0.2\ s$, $t = 10\ s$ and $t = 20\ s$.

material and the thermophysical properties are assumed to be the same in both the solid and liquid phases. The initial temperature of molten steel is 2000 K, which is higher than the melting temperature of 1809 K. We consider Dirichlet boundary condition ($T = 300\ K$) in the left side while homogeneous Neumann boundary condition is considered for all others sides of the computational domain. The thermophysical properties employed for the numerical simulations are summarized Table 3. A uniform mesh with 100×100 cells is used in our computations and the time step $\Delta t = 0.005\ s$ is considered in this section.

Figure 2 presents the time evolution of temperature for both cases without and with radiation at three different instants $t = 0.2\ s$, $10\ s$ and $20\ s$. As it can be seen, the presence of radiation has affected the temperature profile as well as the position of the liquid-solid interface. This can be clearly seen in Figure 3 where

ICCS Camera Ready Version 2022
To cite this paper please use the final published version:
DOI: 10.1007/978-3-031-08751-6_22

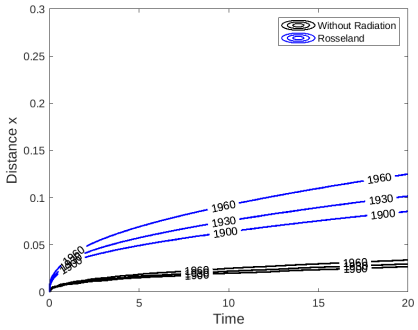

Fig. 4. Temperature contours with and without radiation along for Case 1.

a cross-section of the temperature along the horizontal centerline is displayed for the considered times. Furthermore, to clearly illustrate the effect of radiation on the temperature, Figure 4 shows the isolines corresponding to $T = 1900\ K$, $T = 1930\ K$ and $T = 1960\ K$ for both cases, with and without radiation. As expected, accounting for radiative effects in the solidification process would results in a more accurate results than the radiationless simulations for both the temperature distribution and the interface of the phase change.

4.3 Steel solidification: Case 2

This example is similar to the previous solidification problem during the process of continuous casting of steel. We consider a square $0.2\ m \times 0.2\ m$ material using similar thermophysical properties. However, the boundary conditions in this case are different, where we consider Robbin boundary in all the computational domain boundaries as given by equation (2). The time evolution of temperature for both simulations, with and without radiation is presented in Figure 5 at three different instants $t = 0.2\ s$, $10\ s$ and $20\ s$. As in the previous example, the presence of radiation has affected both, the temperature profile and the position of the liquid-solid interface. This is clearly depicted in Figure 6 where a cross-section of the temperature along the horizontal center-line is plotted. We also present in Figure 7 the isolines corresponding to temperature values of $T = 1000\ K$, $T = 1300\ K$ and $T = 1500\ K$. This figure clearly shows that the presence of radiation affects the temperature distribution and therefore it should not be neglected in phase-change applications that involve high temperature.

5 Conclusions

In this study, we have presented a class of computational techniques for enhancing steel solidification by a nonlinear transient thermal model. The governing equations consist of a nonlinear heat transfer equations with a phase-field

ICCS Camera Ready Version 2022
To cite this paper please use the final published version:
DOI: 10.1007/978-3-031-08751-6_22

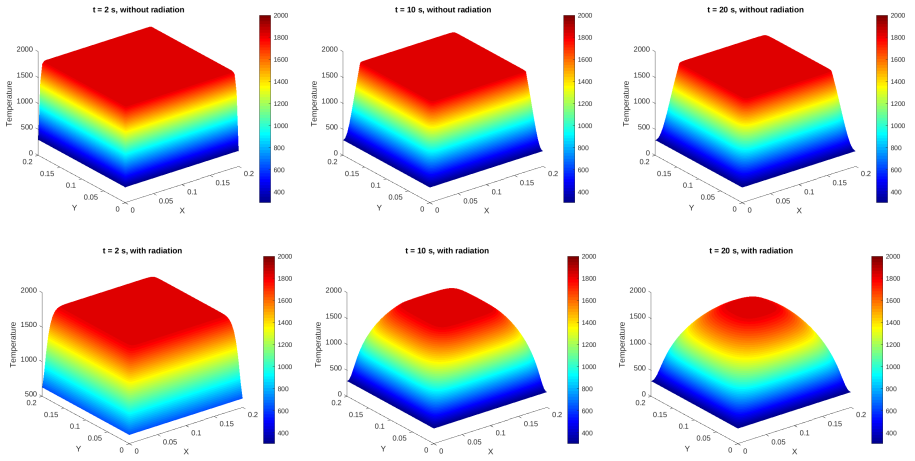

Fig. 5. Temperature without radiation (first row) and with radiation (second row) obtained for Case 2 at time $t = 0.2\ s$ (first column), $t = 10\ s$ (second column) and $t = 20\ s$ (third column).

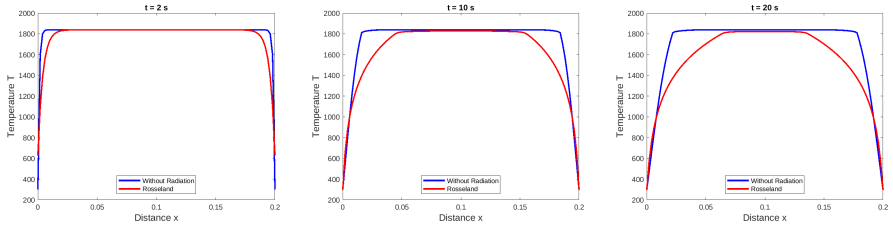

Fig. 6. Cross-sections of the temperature with and without radiation along the horizontal centerline for Case 1 at time $t = 0.2\ s$, $t = 10\ s$ and $t = 20\ s$.

function to account for phase change in the model. The thermal radiation effects are included in the model by using the Rosseland approach for which the phase-change properties appear in the optical parameters of the material. A fully implicit time integration scheme along with a Newton-type algorithm is implemented for the numerical solution of the proposed model to deal with the nonlinear terms. In our numerical simulations, we have used structured meshes for the space discretization. However, the method can also be extended to the use of unstructured meshes based on a similar formulation. Numerical results have been presented for a test example with known exact solution. The method has also been applied for solving two test examples in steel solidification using different diffusion values. The presented results support our expectations for an accurate and stable behaviour for all radiative regimes considered. Future work

ICCS Camera Ready Version 2022
To cite this paper please use the final published version:
DOI: 10.1007/978-3-031-08751-6_22

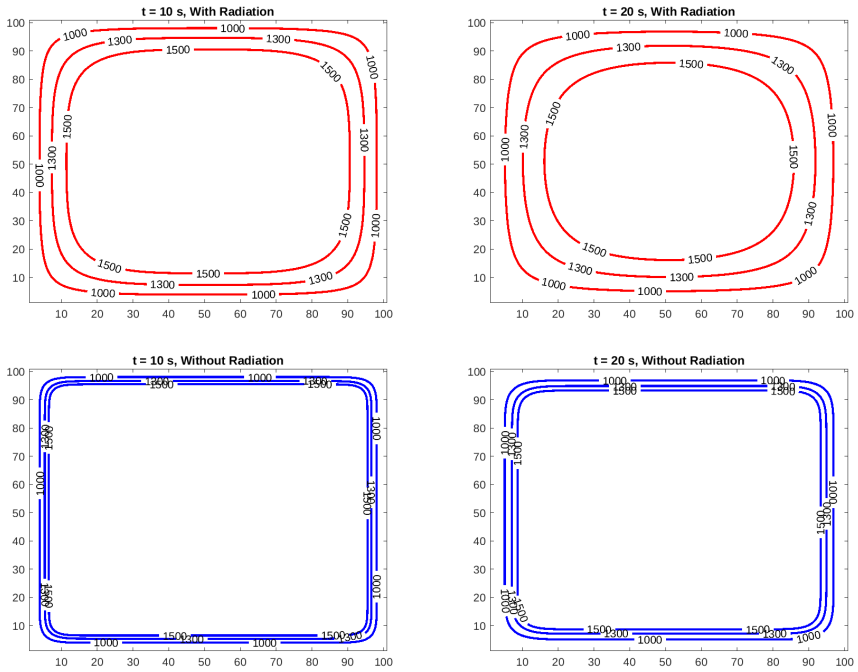

Fig. 7. Temperature contours with and without radiation along for Case 2.

will concentrate on the extension of this method to radiative transfer problems in phase-change domains using full radiative model on unstructured meshes and using high-order spatial discretizations.

Acknowledgements Financial support provided by the Royal Society under the contract IES-R2-202078 is gratefully acknowledged.

References

1. S.K. Choudhary and D. Mazumdar. Mathematical modelling of fluid flow, heat transfer and solidification phenomena in continuous casting of steel. *Steel Research*, 66(5):199–205, 1995.
2. L. Klimeš and J. Štětina. A rapid GPU-based heat transfer and solidification model for dynamic computer simulations of continuous steel casting. *Journal of Materials Processing Technology*, 226:1–14, 2015.
3. S. Koric, L.C. Hibbeler, and B.G. Thomas. Explicit coupled thermo-mechanical finite element model of steel solidification. *International Journal for Numerical Methods in Engineering*, 78(1):1–31, 2009.

ICCS Camera Ready Version 2022
To cite this paper please use the final published version:
DOI: 10.1007/978-3-031-08751-6_22

4. M. El Haddad, Y. Belhamadia, J. Deteix, and D. Yakoubi. A projection scheme for phase change problems with convection. *Computers & Mathematics with Applications*, 108:109–122, 2022.
5. Y. Belhamadia, A. Fortin, and T. Briffard. A two-dimensional adaptive remeshing method for solving melting and solidification problems with convection. *Numerical Heat Transfer, Part A: Applications*, 76(4):179–197, 2019.
6. Y. Belhamadia, A. Kane, and A. Fortin. An enhanced mathematical model for phase change problems with natural convection. *Int. J. Numer. Anal. Model*, 3(2):192–206, 2012.
7. Seid Koric, Lance C. Hibbeler, and Brian G. Thomas. Explicit coupled thermo-mechanical finite element model of steel solidification. *International Journal for Numerical Methods in Engineering*, 78(1):1–31, 2009.
8. Seid Koric and Brian G. Thomas. Thermo-mechanical models of steel solidification based on two elastic visco-plastic constitutive laws. *Journal of Materials Processing Technology*, 197(1):408–418, 2008.
9. T. Roubicek. The stefan problem in heterogeneous media. *Annales de l'Institut Henri Poincaré (C) Non Linear Analysis*, 6(6):481–501, 1989.
10. M. Seaid, A. Klar, and R. Pinnau. Numerical solvers for radiation and conduction in high temperature gas flows. *Flow, Turbulence and Combustion*, 75(1):173–190, 2005.
11. M. Seaid. Multigrid Newton-Krylov method for radiation in diffusive semitransparent media. *Journal of computational and applied mathematics*, 203(2):498–515, 2007.
12. S. Rosseland. *Theoretical Astrophysics. Atomic Theory and the Analysis of Stellar Atmospheres and Envelopes*. Clarendon Press, Oxford, 1936.
13. E.W. Larsen, G. Thömmes, A. Klar, M. Seaid, and T. Götz. Simplified PN approximations to the equations of radiative heat transfer and applications. *Journal of Computational Physics*, 183(2):652–675, 2002.
14. Y. Belhamadia, A. Fortin, and É. Chamberland. Anisotropic mesh adaptation for the solution of the Stefan problem. *Journal of Computational Physics*, 194(1):233–255, 2004.
15. Y. Belhamadia, A. Fortin, and É. Chamberland. Three-dimensional anisotropic mesh adaptation for phase change problems. *Journal of Computational Physics*, 201(2):753–770, 2004.
16. V. Alexiades and A.D. Solomon. *Mathematical Modeling of Melting and Freezing Processes*. CRC Press Taylor & Francis Group, 1993.
17. R. E. White. A numerical solution of the enthalpy formulation of the stefan problem. *SIAM Journal on Numerical Analysis*, 19(6):1158–1172, 1982.
18. Y. Saad and M.H. Schultz. GMRES: A generalized minimal residual algorithm for solving nonsymmetric linear systems. *SIAM Journal on scientific and statistical computing*, 7(3):856–869, 1986.
19. P.N. Brown and Y. Saad. Hybrid Krylov methods for nonlinear systems of equations. *SIAM Journal on Scientific and Statistical Computing*, 11(3):450–481, 1990.
20. Y. Belhamadia. A time-dependent adaptive remeshing for electrical waves of the heart. *IEEE Transactions on Biomedical Engineering*, 55(2):443–452, 2008.

ICCS Camera Ready Version 2022
To cite this paper please use the final published version:
DOI: 10.1007/978-3-031-08751-6_22